

## Research

## SHORT COMMUNICATION

# Increase in External Quantum Efficiency of Encapsulated Silicon Solar Cells from a Luminescent Down-Shifting layer

Keith R. McIntosh<sup>1\*,†</sup>, Gay Lau<sup>1</sup>, James N. Cotsell<sup>1</sup>, Katherine Hanton<sup>1</sup>, Derk L. Bätzner<sup>2</sup>, Fabian Bettiol<sup>3</sup> and Bryce S. Richards<sup>4</sup>

<sup>1</sup>Centre for Sustainable Energy Systems, Australian National University, Canberra, ACT 2600, Australia

<sup>2</sup>Institute of Semiconductor Electronics, RWTH Aachen, 52074 Aachen, Germany

<sup>3</sup>Fluorosolar Systems Ltd., Riverside Centre, U10/148 James Ruse Drive, Parramatta, NSW 2150, Australia

<sup>4</sup>School of Engineering and Physical Sciences, Heriot-Watt University, Edinburgh EH14 4AS, UK

**This paper reports the external quantum efficiency (EQE) of encapsulated screen-printed crystalline silicon solar cells, where the encapsulation includes a layer of luminescent down-shifting (LDS) molecules. At wavelengths less than 400 nm, the inclusion of the LDS molecules increases the EQE from near zero to, at most, 40%. The increase in EQE corresponds to a rise in short-circuit current density of  $0.37 \pm 0.13 \text{ mA/cm}^2$  under the AM1-5g spectrum. Copyright © 2008 John Wiley & Sons, Ltd.**

KEY WORDS: modules; optics; quantum efficiency; luminescence; down shifting

Received 17 June 2008; Revised 22 September 2008

## INTRODUCTION

Ninety-two per cent of photovoltaic modules are currently comprised of encapsulated crystalline silicon (c-Si) solar cells.<sup>1</sup> These modules respond poorly to wavelengths less than 400 nm due to absorption in the encapsulation materials—glass and ethylene vinyl acetate—but some of the loss can be circumvented by including a luminescent down-shifting (LDS) layer. The LDS layer absorbs UV photons before they are absorbed by the encapsulants, and emits longer wavelength photons that transmit through the encapsulants to the cell.

The influence of an LDS layer on a photovoltaic module is best assessed by the measurement of the

module's external quantum efficiency (EQE) with and without the LDS layer. From this data the gain or loss at each wavelength  $\lambda$  can be quantified, and furthermore, the change in the module's short-circuit current density  $\Delta J_{SC}$  can be calculated for any incident spectrum. LDS layers have been assessed by EQE measurements on encapsulated cells manufactured from amorphous silicon (a-Si),<sup>2</sup> cadmium sulphide (CdS) heterojunctions with copper sulfide (Cu<sub>2</sub>S)<sup>2</sup> and cadmium telluride (CdTe),<sup>3–6</sup> and copper indium gallium diselenide (CIGS)<sup>7</sup> substrates. But to our knowledge, an EQE measurement on LDS-encapsulated crystalline silicon (c-Si) cells has not been reported since 1981<sup>8</sup> and has never been converted to  $\Delta J_{SC}$  for terrestrial solar spectra. While LDS-encapsulated c-Si cells have been assessed by a direct measurement of  $\Delta J_{SC}$ ,<sup>9–13</sup> these experiments used a xenon lamp illumination source; being blue weighted, the xenon spectrum leads to a higher  $\Delta J_{SC}$  than would occur

\* Correspondence to: Keith R. McIntosh, Centre for Sustainable Energy Systems, Australian National University, Canberra, ACT 2600, Australia.

†E-mail: KRMcIntosh@gmail.com

under terrestrial solar spectra. Finally, the influence of LDS layers on unencapsulated c-Si cells<sup>2,14–16</sup> and photodiodes<sup>17</sup> has been evaluated, but in most cases the associated gain can predominantly be attributed to a reduction in reflection (due to the refractive index of the LDS layer)<sup>2,14,15</sup> rather than LDS itself; this is particularly true of cells with no anti-reflection coating.<sup>14,15</sup>

In this paper we present the EQE of encapsulated planar silicon solar cells with screen-printed metalisation—a cell design that constitutes ~45% of today's photovoltaic market;<sup>1</sup> the other c-Si cells on the market are textured. The LDS layer consists of polymethyl methacrylate (PMMA) doped with luminescent organic dyes.

## EXPERIMENT

The starting wafers were float-zone boron-diffused silicon with a resistivity of 40  $\Omega$ -cm and a final thickness of ~220  $\mu$ m. The wafers were submitted to a phosphorus diffusion for 30 min to create an emitter with a sheet resistance of either 30 or 70  $\Omega$ /sq. The front surface was then etched in hydrofluoric acid (HF) to remove the phosphorus glass, coated with  $85 \pm 5$  nm of amorphous silicon nitride ( $\text{Si}_x\text{N}_y$ ) by plasma enhanced chemical vapour deposition, and screen printed with silver paste containing 1.5% phosphorus (Ferro 3349) to create fingers of widths around 120  $\mu$ m. After coating the rear surface in screen-print aluminium paste (Ferro 5540), the samples were fired by rapid-thermal anneal in an atmosphere of  $\text{O}_2$  and  $\text{N}_2$  at a peak temperature of ~810°C for 3 s, and then forming-gas annealed at 400°C for 30 min. Finally, cells with an area of  $3.0 \times 3.0$  cm<sup>2</sup> were removed from the wafers using a dicing saw.

This fabrication procedure was chosen to produce devices similar to the multi-crystalline silicon (mc-Si) cells manufactured by many PV companies: the screen-print fingers and  $\text{Si}_x\text{N}_y$  anti-reflection coating on planar silicon provide a similar reflection, and the emitter sheet resistances, which represent lower and upper bounds (30 and 70  $\Omega$ /sq) to that used by industry, provide a similar front-surface recombination. The only parameter that is considerably different to that used in industrial mc-Si cells is the bulk resistance: due to depleted silicon stocks, the cells were fabricated from 40  $\Omega$ -cm rather than ~1  $\Omega$ -cm silicon. But the difference is not relevant to this study because it does

not alter the EQE at the wavelengths affected by the LDS molecules ( $\lambda < 750$  nm).

Figure 1 plots the EQE of the unencapsulated cells with (a) 30  $\Omega$ /sq and (b) 70  $\Omega$ /sq emitters. The beam area was  $2.5 \times 1.5$  mm<sup>2</sup> and directed at the centre of the cell. For a given sheet resistance, the EQEs are nearly identical prior to encapsulation. Table I presents the current–voltage ( $I$ - $V$ ) parameters measured under a xenon flash lamp. The data are included to show that the cells'  $I$ - $V$  parameters are similar to those of industrial cells; we do not use  $I$ - $V$  measurements to quantify  $\Delta J_{\text{SC}}$  induced by LDS because the xenon spectrum is too dissimilar from standard spectra, and

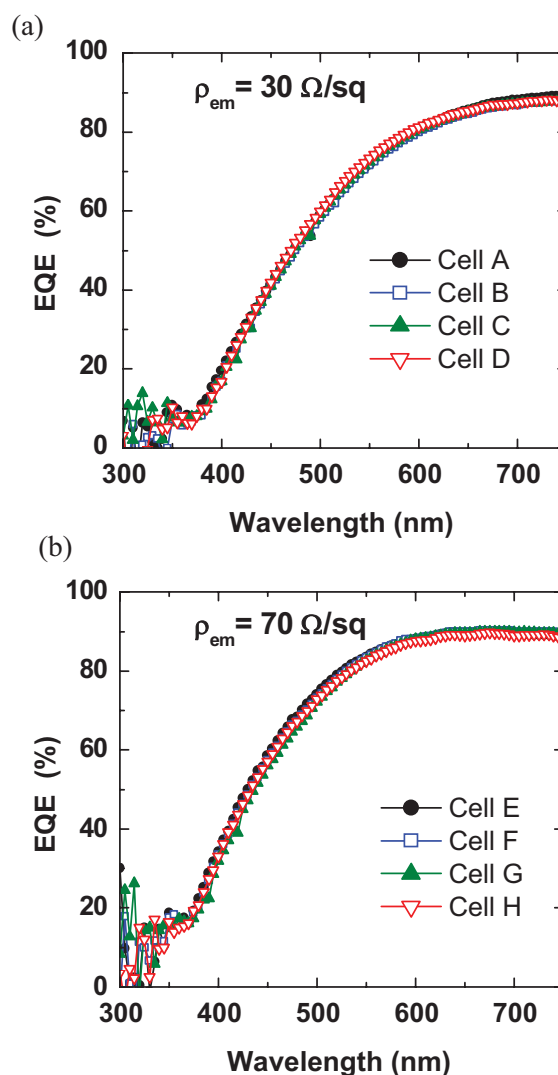


Figure 1. External quantum efficiency (EQE) of unencapsulated cells with (a) 30  $\Omega$ /sq and (b) 70  $\Omega$ /sq emitters

Table I. Current–voltage characteristics of unencapsulated solar cells measured under a xenon flash lamp calibrated to one-sun intensity

Cell	$\rho_{em}$ ( $\Omega\text{-cm}^2$ )	$V_{OC}$ (V)	$J_{SC}$ ( $\text{mA}/\text{cm}^2$ )	$FF$	$\eta$ (%)
A	30	0.607	32.7	0.733	14.6
B	30	0.603	32.2	0.709	13.8
C	30	0.607	32.2	0.741	14.5
D	30	0.607	32.6	0.745	14.7
E	70	0.591	33.2	0.709	13.9
F	70	0.610	32.8	0.725	14.5
G	70	0.602	32.8	0.700	13.8
H	70	0.607	32.9	0.722	14.4

The characteristics are the open-circuit voltage  $V_{OC}$ , short-circuit current density  $J_{SC}$ , fill factor  $FF$  and cell efficiency  $\eta$ .

because the  $I$ – $V$  accuracy is insufficient to detect the small  $\Delta J_{SC}$  calculated from the EQE.

Figure 2 presents a cross-section of the encapsulated cells. The upper layer was cast polymethyl methacrylate (PMMA), often called perspex, and was either undoped or doped with one of three fluorescent organic dyes produced by BASF: LUMOGEN570, LUMOGEN083 or LUMOGEN300.<sup>18</sup> These dyes, based on naphthalomide and perylene molecules, can be photostable over some years<sup>19,20</sup> but may require refining if they are to survive the decades of field exposure required of PV modules. Figure 3 presents the dyes' absorption and emission spectra,<sup>18</sup> where the excitation wavelength for the emission spectra was just below the lowest emission wavelength (approximately 370, 450 and 520 nm, respectively). The dye concentrations in the PMMA were those optimised for *Fluorsolar*<sup>TM</sup> daylighting technology.<sup>21</sup> The PMMA was optically coupled to the solar cells with silicone (Wacker Silgel612), and prior to encapsulation, a metal tab was soldered to the busbar to permit electrical contact to the cell.

The undoped PMMA–silicone encapsulation of this study has similar optical properties to the glass–EVA encapsulation of a conventional solar module: The front-surface reflection is nearly identical because, as shown in Figure 4, PMMA has almost the same refractive index  $n(\lambda)$  as low-iron Starphire glass. And

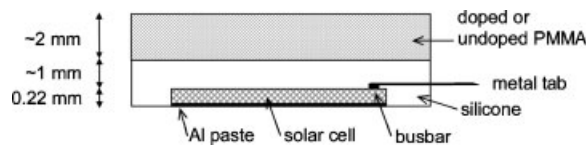


Figure 2. Cross-section of encapsulated cell (fingers not shown)

the absorption loss is similar because the absorption coefficient  $\alpha(\lambda)$  of the undoped PMMA is similar to that of EVA, which is the most absorbing layer of a conventional module. The main difference between the encapsulation structures is that the refractive index of the silicone is lower than the other materials, leading to a small reflection at the PMMA–silicone interface (0.07% at 450 nm) and to slightly more reflection at the silicone– $\text{Si}_x\text{N}_y$  interface (16.9% at 450 nm) as opposed to an EVA– $\text{Si}_x\text{N}_y$  interface (15.9% at 450 nm) for normally incident rays. Consequently, the PMMA–silicone modules of this study would have a slightly higher optical loss than equivalent glass–EVA

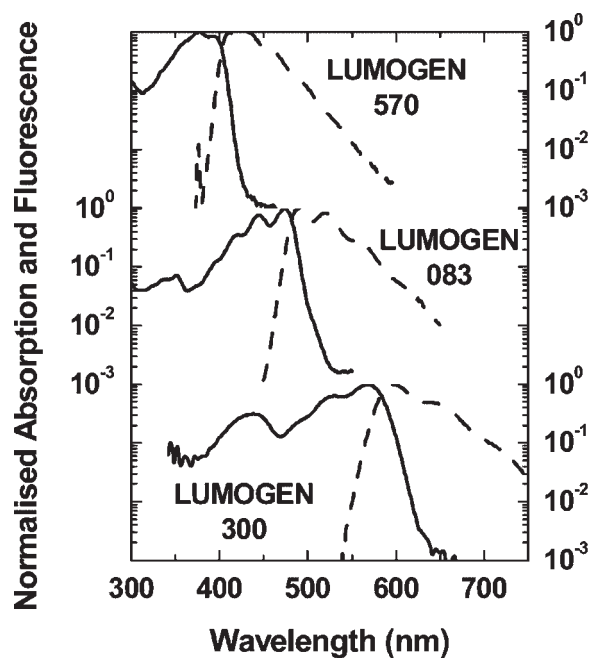


Figure 3. Normalised absorption (solid) and fluorescence (dashed) spectra of LUMOGENs 570, 083 and 300

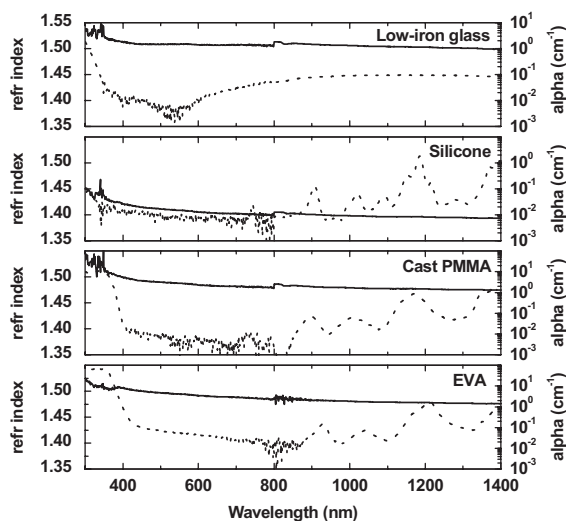


Figure 4. Refractive index (solid) and absorption coefficient (dotted) measured for low-iron Starphire glass, Wacker silgel612 silicone, cast PMMA and EVA

modules. The data of Figure 4 was determined by calculating  $n(\lambda)$  and  $\alpha(\lambda)$  from the measured hemispherical reflection and transmission of planar samples, as outlined in the appendix.

Figure 5 plots the EQE of the encapsulated cells. Like a conventional module, the cells encapsulated by undoped PMMA have a very low EQE at  $\lambda < 400$  nm due to absorption in the encapsulants. At these wavelengths, the EQE is significantly higher for cells encapsulated by doped PMMA, reaching 40% for LUMOGEN570-doped PMMA. The improvement in EQE occurs because photons are absorbed by the LDS molecules prior to being absorbed by the PMMA, and then reemitted at the longer emission wavelengths (see Figure 3) that are not absorbed by the encapsulants.

At most, the EQE at the absorption wavelength can increase to the level of the EQE at the emission wavelength, minus 12.5% for the escape-cone loss. Additional loss occurs due to non-ideal fluorescence quantum yield, self-absorption and absorption in the encapsulants.<sup>22</sup> Edge loss is negligible (<0.3%, assuming uniform emission at all solid angles) because the beam was incident to the centre of the cell.

Thus, it can be construed from Figure 5 that the improvement in EQE induced by LUMOGEN570 is as high as might be expected: at  $\lambda < 400$  nm the EQE is 30–40%, which is not far below the EQE at the emission wavelength of 400–450 nm (see Figure 3). On the other hand, the EQE of the cells encapsulated with LUMOGEN083 and LUMOGEN300 is much

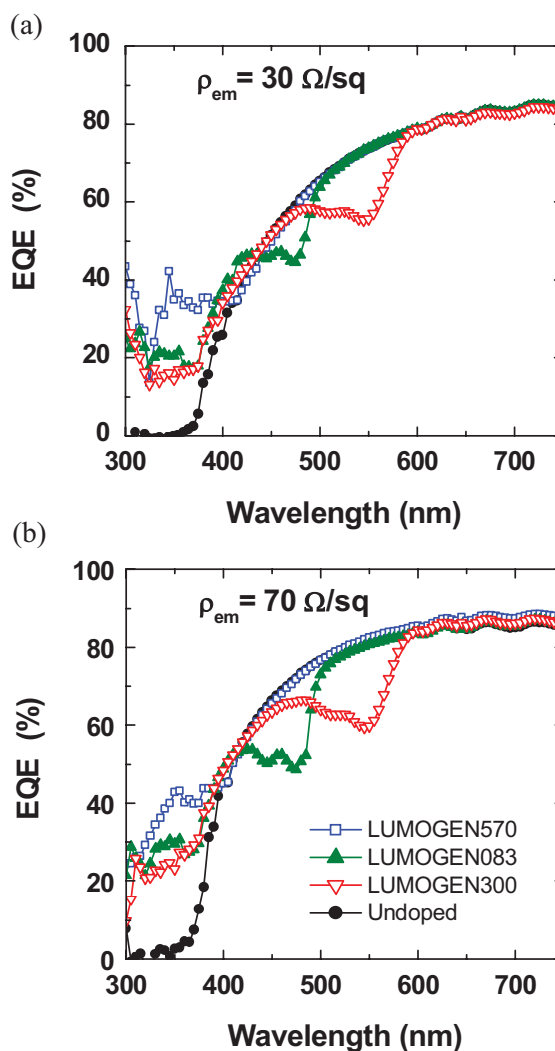


Figure 5. External quantum efficiency of encapsulated cells with (a) 30 Ω/sq and (b) 70 Ω/sq emitters

lower than the EQE at their emission wavelengths, probably due to a combination of their poor absorption coefficient at short wavelengths and to self-absorption. Instead, these LUMOGENs absorb more strongly at longer wavelengths as evident by their influence on the EQE curves of Figure 5. Unfortunately, there is little to be gained from LDS at these wavelengths because the EQE of the cells encapsulated with undoped-PMMA is reasonably high (and not far below the EQE at the possible emission wavelengths). In fact, at some wavelengths the inclusion of the LUMOGENs decreases the EQE because the escape-cone and other losses exceed the gain.

Table II. Change in the short-circuit current  $\Delta J_{sc}$  of the encapsulated cell due to the PMMA dopant

PMMA dopant	Cell ID	Calculated $\Delta J_{sc}$ (mA/cm <sup>2</sup> )		
		AM0	AM1-5g	AM1-5d
Modules using cells with 30 $\Omega$ /sq emitters				
None	A	—	—	—
LUMOGEN570	B	0.50 $\pm$ 0.19	0.29 $\pm$ 0.13	0.20 $\pm$ 0.09
LUMOGEN083	C	0.16 $\pm$ 0.19	0.01 $\pm$ 0.13	−0.05 $\pm$ 0.09
LUMOGEN300	D	−0.35 $\pm$ 0.19	−0.54 $\pm$ 0.13	−0.58 $\pm$ 0.09
Modules using cells with 70 $\Omega$ /sq emitters				
None	E	—	—	—
LUMOGEN570	F	0.56 $\pm$ 0.19	0.37 $\pm$ 0.13	0.27 $\pm$ 0.09
LUMOGEN083	G	−0.26 $\pm$ 0.19	−0.44 $\pm$ 0.13	−0.47 $\pm$ 0.09
LUMOGEN300	H	−0.62 $\pm$ 0.19	−0.85 $\pm$ 0.13	−0.89 $\pm$ 0.09

$\Delta J_{sc}$  calculated from the measured EQE for three spectra weighted to 100 mW/cm<sup>2</sup>. The uncertainty arises from an estimated  $\pm 10\%$  error in the EQE below 400 nm.

To evaluate the LUMOGENs further, Table II lists  $\Delta J_{sc}$  calculated from the difference in EQE of the doped- and undoped-PMMA modules using the equation

$$\Delta J_{sc} = q \int_{300 \text{ nm}}^{700 \text{ nm}} \Phi(\lambda) [\text{EQE}_{\text{doped}}(\lambda) - \text{EQE}_{\text{undoped}}(\lambda)] d\lambda \quad (1)$$

where  $\Phi(\lambda)$  is the incident photon flux of a given spectra. The table presents  $\Delta J_{sc}$  for three standard spectra.<sup>23</sup> The uncertainty in  $\Delta J_{sc}$  results from assuming an error of  $\pm 10\%$  at wavelengths less than 400 nm, which represents the largest standard deviation of five measurements at each wavelength; at wavelengths greater than 400 nm, the illumination of the spectral response instrument was more intense and the standard deviation of the subsequent signal was negligible.

The increase in  $J_{sc}$  is highest for the most blue-weighted spectrum—the AM0 spectrum—because the only increase in EQE occurs at  $\lambda < 400$  nm. And the absolute  $\Delta J_{sc}$  is greater for cells with the higher sheet resistance since their EQE is higher (due to less emitter recombination) at the emission wavelength. The most relevant value of Table II is  $\Delta J_{sc} = 0.37 \pm 0.13$  mA/cm<sup>2</sup> for the 70  $\Omega$ /sq emitter samples under the AM1-5g spectrum; this indicates that the inclusion of LUMOGEN570 at the front of a conventional module would lead to a  $\sim 1\%$  increase in  $J_{sc}$ —and therefore the relative efficiency—of a conventional module under standard test conditions. This figure compares to 0.7 mA/cm<sup>2</sup> predicted by ray tracing simulation for similar samples when the LDS layer is included between glass and EVA.<sup>22</sup> The lower

experimental value presented here may have arisen from some UV photons being absorbed in the PMMA before they could be absorbed by LDS molecules, from a higher concentration of LUMOGENs causing more self-absorption, from a lower fluorescent quantum yield than used in the simulation (93%), or from the reflection of oblique rays at the PMMA–silicone interface.

The same experiment was conducted on similarly prepared cells with a sheet resistance of 60  $\Omega$ /sq. When encapsulated, the samples exhibited similar changes in EQE to those in Figure 5. In particular, the LDS dyes caused an increase in EQE at short wavelengths from 0 to 40  $\pm 5\%$  for LUMOGEN570, from 0 to 35  $\pm 5\%$  for LUMOGEN083 and from 0 to 35  $\pm 5\%$  for LUMOGEN300.  $\Delta J_{sc}$  was not calculated for these samples, however, since the pre-encapsulated EQE of the cells did not overlap like those in Figure 1, preventing an accurate comparison at wavelengths more than 400 nm.

Finally, we comment on the application of LUMOGENs to modules containing high-efficient silicon solar cells. Such cells have a considerably superior quantum efficiency (at all wavelengths) than the cells of this study due to surface texture and lower recombination rates. If high-efficient cells—rather than low-efficient cells—had been used in this experiment, a higher  $\Delta J_{sc}$  would have resulted from the LUMOGEN570 module. This is because LUMOGEN570 absorbs photons at wavelengths where the module's EQE would otherwise be 0% due to absorption in the PMMA (or EVA), and down-shifts them to 400–450 nm, where the high-efficient cells have a superior EQE to the low-efficient cells of this

study. For example, a gain of +2% would be expected for a SunPower A-300 solar cell<sup>24</sup> because its EQE at 400 nm is approximately twice that of the low-efficient cells.

In contrast, a lower  $\Delta J_{SC}$  would have resulted if high-efficient cells had been incorporated into the LUMOGEN083 and LUMOGEN300 modules. A lower gain (or a more negative gain) is expected for high-efficient cells because their EQE at the dyes' absorption wavelengths is not far below that at the emission wavelengths; thus, the losses associated with the LDS would outweigh any gains from the higher EQE at longer wavelength. A detailed study into the application of LUMOGENs to high-efficient silicon modules is underway.

## CONCLUSION

This paper presented the EQE of modern silicon solar cells encapsulated by PMMA. A substantial increase in EQE was observed at wavelengths less than 400 nm when the PMMA was doped with BASF's LUMOGEN organic dyes compared to when the PMMA was undoped. In the case of LUMOGEN570, the improved EQE correlated to a rise in  $J_{SC}$  of  $0.37 \pm 0.13 \text{ mA/cm}^2$  under the AM1-5g spectrum, which equates to an increase of  $\sim 1\%$  in the relative efficiency of the module. A similar increase in  $J_{SC}$  is expected for a conventional mc-Si module if the same doped PMMA were coated to its front surface; the  $J_{SC}$  might be increased by an optimisation of the dye concentration. Should the PMMA coating not prove robust under weathering, most of the benefit of the LDS layer could be attained by coating LUMOGEN-doped PMMA to the inside of the glass, or by using a LUMOGEN-doped EVA,<sup>25</sup> in such case, absorption in the low-iron glass reduces the gain in  $J_{SC}$  by  $0.06 \text{ mA/cm}^2$  (as calculated for the AM1-5g spectrum using  $a(\lambda)$  from Figure 4). It remains to be evaluated whether the optical gain outweighs the manufacturing cost of incorporating LUMOGENs into a conventional PV module, and whether the LUMOGENs' photostability can be maintained over the operating lifetime of a PV module.

## Acknowledgements

The authors thank Alan Yee and Kian Chin at the University of NSW for their assistance with the quantum efficiency measurements, and Anna Samoc and Marek Samoc at the Research School of Physical Sciences & Engineering at the ANU for assistance

with the reflection and transmission measurements. This work was supported by a grant from BASF (Ludwigshafen, Germany).

## REFERENCES

- Hirshman WP, Hering G, Schmela M. Gigawatts—the measure of things to come. *Photon International* 2007; **3-2007**: 136–166.
- Hovel HJ, Hodgson RT, Woodall JM. The effect of fluorescent wavelength shifting on solar cell spectral response. *Solar Energy Materials* 1979; **2**: 19–29.
- Maruyama T, Kitamura R. Transformations of the wavelength of the light incident upon CdS/CdTe solar cells. *Solar Energy Materials and Solar Cells* 2001; **69**: 61–68.
- Maruyama T, Kitamura R. Transformations of the wavelength of the light incident upon solar cells. *Solar Energy Materials and Solar Cells* 2001; **69**: 207–216.
- Hong BC, Kawano K. PL and PLE studies of KMgF<sub>3</sub>:Sm crystal and the effect of its wavelength conversion on CdS/CdTe solar cell. *Solar Energy Materials and Solar Cells* 2003; **80**: 417–432.
- Hong BC, Kawano K. Organic dye-doped thin films for wavelength conversion and their effects on the photovoltaic characteristics of CdS/CdTe solar cell. *Japanese Journal of Applied Physics* 2004; **43**(4A): 1421–1426.
- Glaeser GC, Rau U. Improvement of photon collection in Cu(In,Ga)Se<sub>2</sub> solar cells and modules by fluorescent frequency conversion. *Thin Solid Films* 2007; **515**: 5964–5967.
- Sarti D, Le Poull F, Gravisse P. Transformation du rayonnement solaire par fluorescence: application à l'encapsulation des cellules. *Solar Cells* 1981; **4**: 25–35.
- Nakata R, Hashimoto N, Kawano K. High-conversion-efficiency solar cell using fluorescence of rare-earth ions. *Japanese Journal of Applied Physics* 1996; **35**: L90–L93.
- Jin T, Inoue S, Machida K, Adachi G. Photovoltaic cell characteristics of hybrid silicon devices with lanthanide complex phosphor-coating film. *Journal of the Electrochemical Society* 1997; **144**(11): 4054–4058.
- Jin T, Inoue S, Tsutsumi S, Machida K, Adachi G. High conversion efficiency photovoltaic cell enhanced by lanthanide complex phosphor film coating. *Chemistry Letters* 1997; **2**: 171–172.
- Maruyama T, Bandai J. Solar cell module coated with fluorescent coloring agent. *Journal of the Electrochemical Society* 1999; **146**(12): 4406–4409.
- Maruyama T, Enomoto A, Shirasawa K. Solar cell module colored with fluorescent plate. *Solar Energy Materials & Solar Cells* 2000; **64**: 269–278.
- Maruyama T, Shinyashiki Y. Solar cells coated with fluorescent coloring agent. *Journal of the Electrochemical Society* 1998; **145**(8): 2955–2957.

15. Maruyama T, Shinyashiki Y, Osako S. Energy conversion efficiency of solar cells coated with fluorescent coloring agent. *Solar Energy Materials and Solar Cells* 1998; **56**: 1–6.
16. Švrček V, Slaoui A, Muller JC. Silicon nanocrystals as light converter for solar cells. *Thin Solid Films* 2004; **451–452**: 384–388.
17. Garbuzov DZ, Forrest SR, Tsekoun AG, Burrows PE, Bulović V, Thompson ME. Organic films deposited on Si p-n junctions: accurate measurements of fluorescence internal efficiency, and applications to luminescent anti-reflection coatings. *Journal of Applied Physics* 1996; **80**(8): 4644–4648.
18. BASF Lumogen F organic dye data sheets, [http://www.performancechemicals.basf.com/ev-wcms-in/internet/en\\_GB/portal/show-content\\_cps/function:evproducts/multilist/basic/4704/4732](http://www.performancechemicals.basf.com/ev-wcms-in/internet/en_GB/portal/show-content_cps/function:evproducts/multilist/basic/4704/4732), last accessed 17 December 2007.
19. Seybold G, Wagenblast G. New perylene and violanthrone dyestuffs for fluorescent collectors. *Dyes and Pigments* 1989; **11**(4): 303–317.
20. Murphy J. *Additives for Plastics Handbook* (2nd edn). Elsevier Science Ltd: Oxford, 2001; 64.
21. Smith GB, Franklin JB. Sunlight collecting and transmitting system, U.S. Patent 6,059,438, 2000.
22. McIntosh KR, Richards BS. Increased mc-Si module efficiency using fluorescent organic dyes: a ray-tracing study. *Proceedings of the 4th World Conference on Photovoltaic Energy Conversion (IEEE)*, 2006; 2108–2111.
23. ASTM standards E-490-00, E-891 and E-892, available at <http://tredc.nrel.gov/solar/spectra/>, last accessed 17 December 2007.
24. Mulligan WP, Rose DH, Cudzinovic MJ, De Ceuster DM, McIntosh KR, Smith DD, Swanson RM. Manufacture of solar cells with 21% efficiency. *Proceedings of the 19th European Photovoltaic Solar Energy Conference*, Paris, 2004; 387–390.
25. Richards BS, Boehm A. Enhancing the performance of photovoltaic modules via luminescent down-shifting encapsulation layers, *European Patent Application*, 2007.
26. Hecht E. *Optics* (2nd edn), Chapter 4. Addison–Wesley: New York, 1987.

## APPENDIX

The measured hemispherical reflection  $R_m$  and transmission  $T_m$  were used to calculate the real refractive index  $n$  and absorption coefficient  $\alpha$  of several semitransparent samples—the results of which are plotted in Figure 4. Assuming the samples to be specular with parallel sides

$$R_m = R \left[ \frac{1 + (1 - A)^2(1 - 2R)}{1 - (1 - A)^2R^2} \right] \text{ and} \quad (2)$$

$$T_m = \frac{(1 - R)^2(1 - A)}{1 - (1 - A)^2R^2} \quad (3)$$

where  $R$  is the reflection at each air–sample interface and  $A$  is the fraction of light absorbed per pass. These equations can be derived by tracing a ray through a sample and taking an infinite sum of the ray's intensity that exits the illuminated ( $R_m$ ) and non-illuminated ( $T_m$ ) sides. Solving Equations (2) and (3) simultaneously provides  $R$  and  $A$ , from which  $n$  and  $\alpha$  can be calculated using<sup>26</sup>

$$n = \frac{1 + \sqrt{R}}{1 - \sqrt{R}} \text{ and} \quad (4)$$

$$\alpha = \frac{\ln(1 - A)}{W} \quad (5)$$

where  $W$  is the sample thickness. Both equations assume the ray travels perpendicular to the sample, although in practise, the angle of incidence was  $8^\circ$ . This angle has negligible influence on the calculation of  $n$  from  $R$  for randomly polarised light.<sup>26</sup> It does, however, have a small influence on the calculation of  $\alpha$  because for each pass through the sample the ray travels a distance  $W/\cos(\theta_t)$  rather than  $W$ , where  $\theta_t$  is the transmission angle calculated from Snell's law and  $n$ . The data plotted in Figure 4 has accounted for this small factor (just 1.004 for  $n = 1.5$ ).